Braun's lipoprotein facilitates OmpA interaction with the *E. coli* cell wall

Firdaus Samsudin,[1] Alister Boags,[1] Thomas J. Piggot,[1,2] and Syma Khalid[1,#]

[1]School of Chemistry, University of Southampton, Highfield, Southampton, UK

[2]CBR Division, Defence Science and Technology Laboratory, Porton Down, Salisbury, Wiltshire, UK

[#]To whom correspondence should be addressed. e-mail: S.Khalid@soton.ac.uk

Summary

Gram-negative bacteria such as *E. coli* are protected by a complex cell envelope. The development of novel therapeutics against these bacteria necessitates a molecular level understanding of the structure-dynamics-function relationships of the various components of the cell envelope. We use atomistic molecular dynamics simulations to reveal the details of covalent and non-covalent protein interactions that link the outer membrane to the aqueous periplasmic region. We show that the Braun's lipoprotein tilts and bends, and thereby lifts the cell wall closer to the outer membrane. Both monomers and dimers of the outer membrane porin OmpA can interact with peptidoglycan in the presence of Braun's lipoprotein, however in the absence of the latter, only dimers of OmpA show a propensity to form contacts with peptidoglycan. Our study provides a glimpse of how the molecular components of the bacterial cell envelope interact with each other to mediate cell wall attachment in *E. coli.*

Introduction

The cell envelope of *E. coli* is composed of two membranes separated by a region known as the periplasm or the periplasmic space (Silhavy et al. 2010). The outer membrane (OM) is composed of lipopolysaccharide (LPS) molecules in the outer leaflet and a mixture of phospholipids, both zwitterionic and anionic, in the inner leaflet (Lugtenberg & Peters 1976). Proteins that are integral to this membrane are almost invariably beta barrels in architecture (Tsirigos et al. 2011). The periplasm contains the sugar-peptide polymer, peptidoglycan (PGN), as well as many different periplasmic proteins. The

PGN network is attached to the OM and the IM via both covalent and non-covalent interactions (Vollmer et al. 2004; Vollmer & Bertsche 2008; Vollmer et al. 2008).

The only known protein that provides a covalent link to PGN is Braun's lipoprotein (BLP, also known as Lpp and murein lipoprotein), which is one of the most abundant proteins in *E. coli* (Braun & Wolff 1970; Braun 1975). BLP is anchored in the OM via a lipidated N-terminus, while the C–terminus is covalently attached to the peptide chain of PGN. BLP exists in PGN-bound and PGN-unbound states, with the former representing around one third of the population (Braun & Sieglin 1970; Inouye et al. 1972; Bosch & Braun 1973; Lee & Inouye 1974). Crystallographic data revealed that the *E. coli* BLP forms a stable homotrimer with a tight coiled coil motif held together by an alanine zipper unit (Shu et al. 2000). Recently, electron microscopy and electron cryomicroscopy studies showed that the length of BLP has a direct influence on the distance between the peptidoglycan layer and the outer membrane of *E. coli* (Cohen et al. 2017). However, how the BLP trimer is positioned with respect to the OM and the PGN network, remains unknown at the individual molecule level.

In addition to the covalent linkage provided by BLP, PGN is also attached non-covalently to several OM and IM proteins such as OmpA-like domains (Koebnik 1995), PGN-associated lipoproteins (PALs) (Parsons et al. 2006), and flagella motor proteins (Roujeinikova 2008). The *E. coli* outer membrane porin OmpA is a multi-domain protein whose N-terminal domain (NTD) is

made of a beta barrel and C-terminal domain (CTD) is a globular periplasmic unit that binds to PGN, connected by an unstructured 20-residue linker region (Smith et al. 2007). The NTD has been subject to numerous functional and structural studies (Pautsch & Schulz 1998; Bond et al. 2002; Arora et al. 2001; Arora et al. 2000; Khalid et al. 2008), while the structure of the CTD has recently emerged from a nuclear magnetic resonance (NMR) study (Ishida et al. 2014). Several experimental evidence suggest that the full-length OmpA can form a homodimer (Stenberg et al. 2005; Zheng et al. 2011), the model of which has been proposed and validated by mass spectrometry and molecular dynamics (MD) simulations (Marcoux et al. 2014; Ortiz-Suarez et al. 2016; Samsudin et al. 2016). The mechanism of PGN attachment to OmpA CTD has been elucidated by crystal structures of a homolog from *Acinetobacter baumannii* bound to a short PGN peptide (Park et al. 2012).

While BLP and OmpA, and their interactions with PGN, have been extensively studied individually and it is likely that both of these proteins form simultaneous interactions with the PGN network *in vivo*, very little is known about any interaction between the two proteins as the spatial arrangement of both proteins within the cell envelope is still largely unexplored at a resolution of individual molecules. Based on the X-ray structures, each helix of the BLP trimer is around 80 Å in length (Shu et al. 2000). If this represents the separation of the OM and the PGN layer, the OmpA linker would have to be fully extended to allow for CTD interaction with PGN. Such a conformation, however, is likely to be entropically unfavourable. Further studies including both proteins in the same environment are therefore crucial to understand the

balance between covalent and non-covalent bonding between the OM and the PGN cell wall.

To this end, here we built atomistic models representing a portion of the *E. coli* cell envelope; namely the OM and the periplasm containing PGN, BLP, and OmpA. Unlike our previous study, the PGN sheet was positioned approximately 90 Å from the lower leaflet of the OM, unbound to the OmpA CTD, allowing us to examine how the latter can interact with PGN in the presence of BLP. This distance was chosen, as it is the length of fully extended, unkinked BLP. Our simulations show that BLP lifts the PGN layer upwards by tilting and bending its helices. This in turn reduces the gap between the OM and the cell wall, thereby facilitating the initial contact between the OmpA CTD and PGN, especially in its monomeric form. OmpA dimers on the other hand are able to interact with the cell wall even in the absence of BLP by extending their linker domain. We also identify interactions between BLP and OmpA as well as showing the interaction of the latter with the cell wall.

Methods

The models. The full length OmpA monomer and dimer models were obtained from Carol Robinson (Marcoux et al. 2014); their structural stability in a model OM has been verified in our previous work (Ortiz-Suarez et al. 2016; Samsudin et al. 2016). The OM model was asymmetric: the upper leaflet was made entirely of full-rough Ra LPS lipids of the R1 core type (Vinogradov et al. 1999; Appelmelk et al. 1994), whereas the lower leaflet comprised a

mixture of phospholipids, i.e. 90% 1-palmitoyl 2-cis-vaccenic phosphatidylethanolamine (PVPE), 5% 1-palmitoyl 2-cis-vaccenic phosphatidylglycerol (PVPG), and 5% 1-palmitoyl 2-cis-vaccenic 3-palmitoyl 4-cis-vaccenic diphosphatidylglycerol (DPG, otherwise known as cardiolipin) (Lugtenberg & Peters 1976; Aibara et al. 1972; Kito et al. 1975; Yokota et al. 1980). This OM model has been validated in our previous simulations studies (Ortiz-Suarez et al. 2016; Samsudin et al. 2016; Piggot et al. 2011). The OmpA structure was inserted into the OM model using g_membed (Wolf et al. 2010) following the procedure previously described (Samsudin et al. 2016).

A PGN network consisting of three strands of ten repeating NAG-NAM-peptide units was constructed and positioned approximately 90 Å from the surface of the lower leaflet of the OM. The BLP homotrimer was built based on the structure from Shu et. al. (Shu et al. 2000) (PDB ID: 1EQ7) with the last residues on both the N- and C-termini manually added back using PyMOL (DeLano 2002). The N-terminus was in turn attached to the tripalmitoyl-S-glyceryl-cysteine (TPGC) residues to incorporate the BLP to the inner leaflet of the OM. The parameters for TPGC were constructed from the standard GROMOS 54A7 force field (Schmid et al. 2011) with the GROMOS 53A6$_{OXY}$ (Horta et al. 2011) ether parameters used for the linkage region. PGN was then covalently linked to the lysine on one of the C-termini of the BLP trimer via its m-DAP residue. The linkage was constructed using the standard GROMOS 54A7 parameters.

Atomistic MD simulations. All simulations were performed using the

GROMACS 5 code (Abraham et al. 2015), the GROMOS 54A7 force field (Schmid et al. 2011) with the SPC water model (Berendsen et al. 1981). Each simulation was run for 100 ns, and at least one independent repeat of each simulation was performed, giving at least 200 ns for each system simulated. Temperatures of 310 K and 323 K were maintained using the velocity rescale thermostat (Bussi et al. 2007) using a time constant of 1 ps. The pressure was maintained semi-isotropically at 1 atm using the Parrinello-Rahman barostat (Parrinello & Rahman 1981) with a time constant of 1 ps. All bonds were constrained using the LINCS algorithm (Hess et al. 1997) to allow for an integration time step of 2 fs. Long-range electrostatics were described using the particle mesh Ewald (PME) method (Essmann et al. 1995). The short-range electrostatic cutoff used was 1.2 nm and the short-range Van der Waals cutoff was also 1.2 nm.

Short equilibration simulations were performed for each system in both the NVT and the NPT ensembles. The NVT equilibration was first run for 500 ps, followed by the NPT equilibration for another 1 ns, after which the pressure of the systems reached a plateau. No positional restraints were imposed on the proteins during these simulations. These equilibration simulations utilized the same thermostat and barostat as mentioned above.

Results

Simulation systems

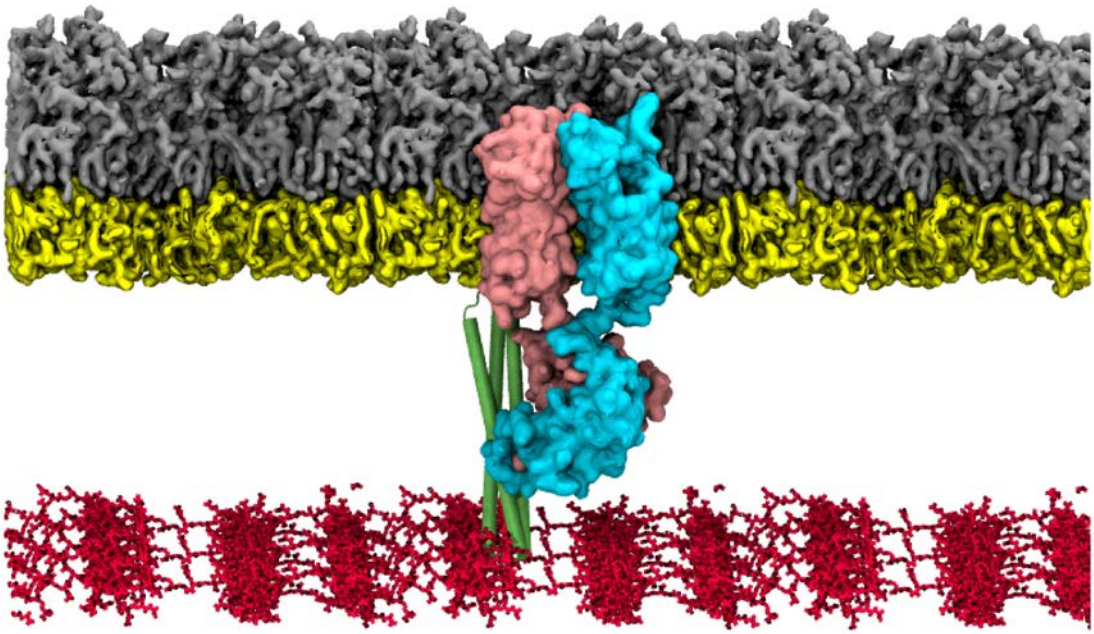

Figure 1 | Simulation setup. A snapshot of a simulation system with the full-length OmpA dimer (cyan and pink), BLP trimer (green), and PGN network (red). OmpA and BLP are embedded within an asymmetric bilayer containing Ra LPS in the upper leaflet (grey), and a mixture of phospholipids in the lower leaflet (yellow).

Table 1 Summary of simulations performed.

System	OmpA	BLP	Temperature (K)	Duration (ns)	OmpA contact with PGN
Control	No	Yes	310	2 x 100	-
Control	No	Yes	323	2 x 100	-
1	Monomer	Yes	310	2 x 100	Yes
1	Monomer	Yes	323	2 x 100	Yes
2	Monomer	No	310	2 x 100	No

2	Monomer	No	323	2 x 100	No
3	Dimer	Yes	310	2 x 100	Yes
3	Dimer	Yes	323	2 x 100	Yes
4	Dimer	No	310	2 x 100	Yes
4	Dimer	No	323	2 x 100	Yes

Four atomistic simulation systems were constructed as described in Table 1 and Figure 1, containing either the full-length OmpA monomer or dimer (Marcoux et al. 2014), in the presence or absence of BLP (Shu et al. 2000). One system of only the BLP trimer in the absence of OmpA was also built as a control. The OmpA NTD was inserted into a biologically relevant model of the OM (Lugtenberg & Peters 1976; Aibara et al. 1972; Kito et al. 1975; Yokota et al. 1980) described in the Methods section. The binding of PGN to OmpA CTD occurs in a non-covalent fashion mediated by two residues, D241 and R256 in *E. coli* OmpA, as indicated by recent crystallographic data (Park et al. 2012) and a simulation study (Samsudin et al. 2016). These residues, however, are located deep within the OmpA CTD, suggesting that it is likely that other residues on the surface of the protein might be involved in initial binding. We therefore started all of our simulations with the CTD of OmpA positioned around 30 Å above a mesh of PGN network to observe the initial binding event. In the presence of BLP, the C-terminus of one of the BLP trimer was covalently linked to a PGN peptide chain. For systems with both OmpA and BLP, they were separated by around 30 Å at the beginning of the simulations. Two independent simulations of each system, each for 100 ns, were performed at 310 K and 323 K; the two temperatures were used as a

means to enhance sampling with independent simulations. One simulation for the systems containing OmpA dimer (System 3 and 4) at 310 K was extended to 500 ns (Figure S1), although we did not observe any significant changes after the first 100 ns. Therefore for simplicity, all analyses were performed using the 100 ns simulations at the two temperatures mentioned in Table 1.

BLP tilts and kinks with respect to the membrane. At the beginning of the simulations, BLP was positioned at a right angle with respect to the plane of the membrane. Intriguingly, at the end of all simulations the BLP helices were observed to tilt, the degree of which was dependent on the presence of OmpA (Fig. 2A). We measured the distribution of BLP tilt angle, and found that in the absence of OmpA BLP stabilized at around 80°, whereas in the presence of OmpA monomer the BLP tilted slightly more at approximately 75°. Adding OmpA dimer to the system resulted in BLP tilted even more at about 65°, suggesting that the BLP helices can flexibly adjust their orientation with respect to the plane of the membrane to adapt to other nearby proteins.

Inspecting the shape of the BLP trimer, we also found that each helix kinked with respect to its helical axis (Fig. 2B). These helix kinks were most prominent on the C-terminal end of the BLP helices, which bent to around 30°. While most helix kinks can be attributed to the presence of certain residues like proline and glycine (Barlow & Thornton 1988; Langelaan et al. 2010; Deville et al. 2008), we could not however find these residues on BLP. The position of the kink on each of the three helices also differed slightly, with helix 1 and 3 showing most bending around residue Y55, which was not the

case with helix 2 (Fig. S2). Despite these different bending properties, BLP remains stable as a trimer throughout the entire simulations. Taken together, these BLP helix kinks and tilts resulted in a lift of the PGN network closer to the OM, effectively closing the gap between PGN and OmpA CTD.

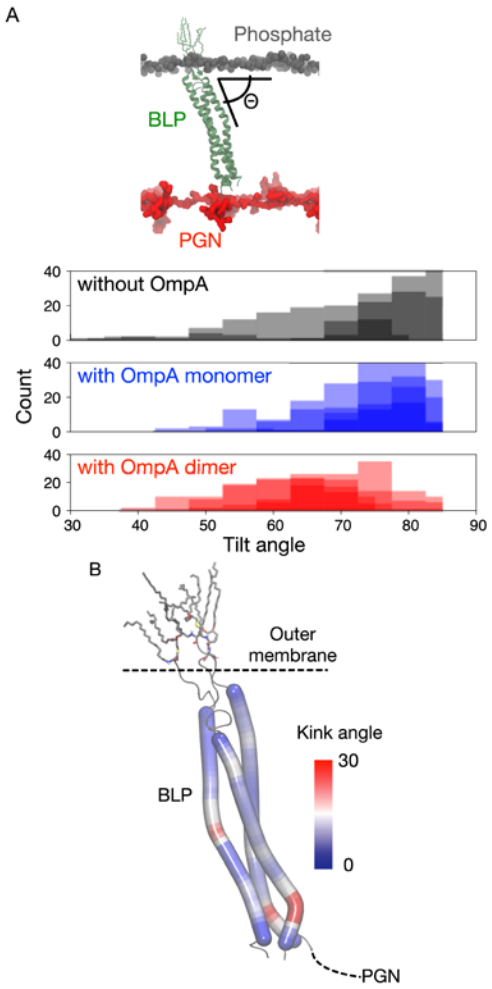

Figure 2 | BLP tilting and bending. (A) The distribution of BLP tilt angle throughout the 100 ns simulations for systems without OmpA (black), with OmpA monomer (blue), and with OmpA dimer (red). This is measured as the acute angle between the centers of geometry of the phosphorus atoms in the inner leaflet of the OM, the N-terminal residues of the BLP, and its C-terminal residues (illustrated at the top of the graph). Independent repeats were plotted separately, and a bin size of 5 degree was used. (B) BLP helix kink angles

calculated along each of the three helices using VMD Bendix plugin (Dahl et al. 2012). The figure shows the final snapshot of BLP from one of the BLP only simulations, coloured based on the degree of helix kink.

BLP facilitates interactions of OmpA monomer with PGN. Our previous simulations showed that the OmpA CTD in its monomeric state has a high propensity to interact with the OM (Samsudin et al. 2016). If such interaction occurs *in vivo* with PGN bound to the CTD, it would cause a severe distortion to the PGN network. Missing from our previous model, however, is BLP that can potentially maintain the PGN within a certain distance from the OM and therefore avoid such distortions. To understand how OmpA monomer behaves in the presence of BLP, we started our simulations with the OmpA CTD unbound from the PGN in the presence of one copy of the BLP trimer.

We found the distance between the OmpA CTD and the surface of the PGN network was reduced during equilibration simulations, and in all four subsequent independent production runs, the CTD contacted the PGN surface (Figs. 3A and 3B). The BLP tilting and bending shifted the PGN layer towards the OmpA CTD, and concomitantly resulted in their interactions. The gap between the PGN layer and the OM was reduced to around 70 Å at the end of the simulations (Fig. 3C). This upward movement of the PGN network therefore eased its interactions with the OmpA monomer. Initial examination of the contact interface pointed towards a group of basic and polar residues, specifically K294, Q295, and R296, on the OmpA CTD that interacted with the

negatively charged glycan moieties. This implies that the initial binding of OmpA to PGN is mediated by a long-range electrostatic force.

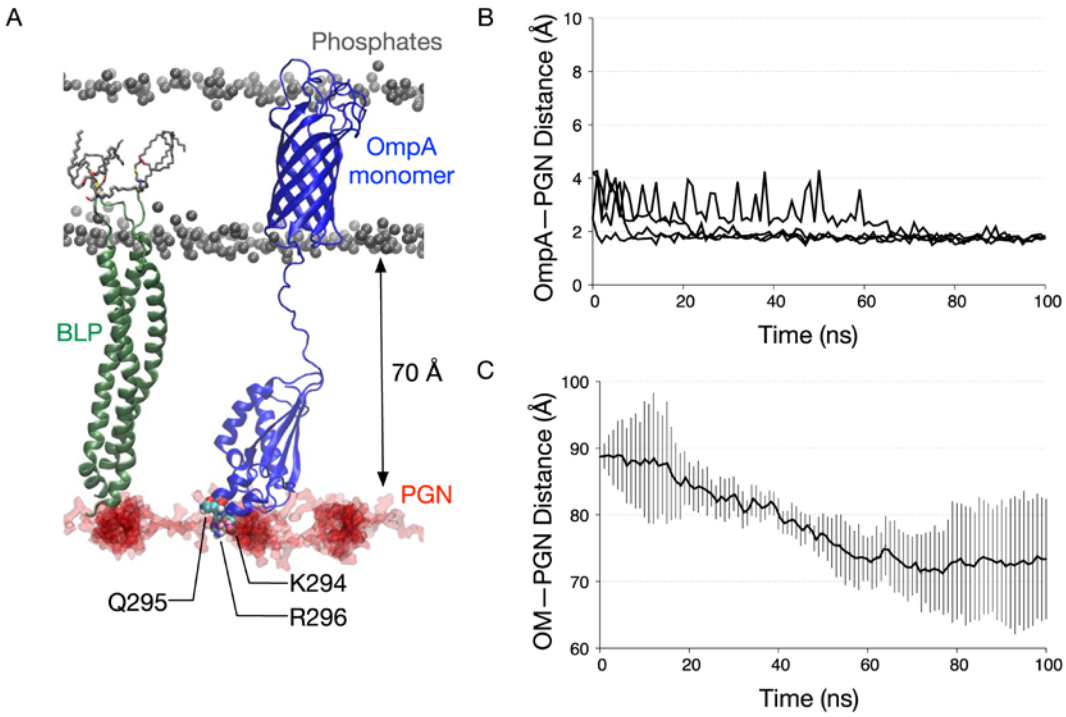

Figure 3 | OmpA monomer interactions with PGN. (A) A snapshot at the end of one of the simulations of OmpA monomer (blue) in the presence of BLP (green), highlighting the interactions of the CTD with the PGN network (red). Residues involved in PGN contacts illustrated in van der Waals representation. **(B)** Minimum distance between OmpA CTD and the PGN network for all four simulations of OmpA monomer with BLP. **(C)** Distance between the PGN network and the OM measured along the z-axis between the centers of geometry of the PGN sugar strands and the phosphorus atoms on the lower leaflet of the OM. This is averaged over all four independent simulations and the error bars indicate standard deviations.

We then repeated these analyses with a similar system without the BLP trimer. Interestingly, we found in all simulations the linker region connecting the OmpA NTD and CTD contracted relative to the original starting conformation, resulting in a binding to the lower leaflet of the OM instead of PGN (Figs. 4A and 4B). In contrast to the simulations with BLP, the distance along the z-axis between the PGN network and the OM remained at around 90 Å (Fig. 4C). This observation is in agreement with Samsudin et. al., which demonstrated a similar linker contraction and membrane binding event of the OmpA monomer.

Samsudin et. al simulations also revealed that the binding of OmpA CTD to the OM is mediated by residues 270-300, which intriguingly include the three key residues for initial interactions with PGN in the presence of the BLP. As this region is highly positively charged, we would expect it to form interactions with a negatively charged surface. This could either be the PGN layer underneath or the phosphate groups of the OM. Our simulations suggest that the latter is a more likely option in the absence of the BLP, perhaps due the large energetic cost for the linker to extend and usher the CTD towards the underlying PGN network. The presence of BLP, however, lowers this energetic cost by reducing the distance between the PGN network and the CTD, making their interactions more likely to occur. Our data therefore illustrate how BLP facilitates initial binding of the OmpA monomer to the cell wall.

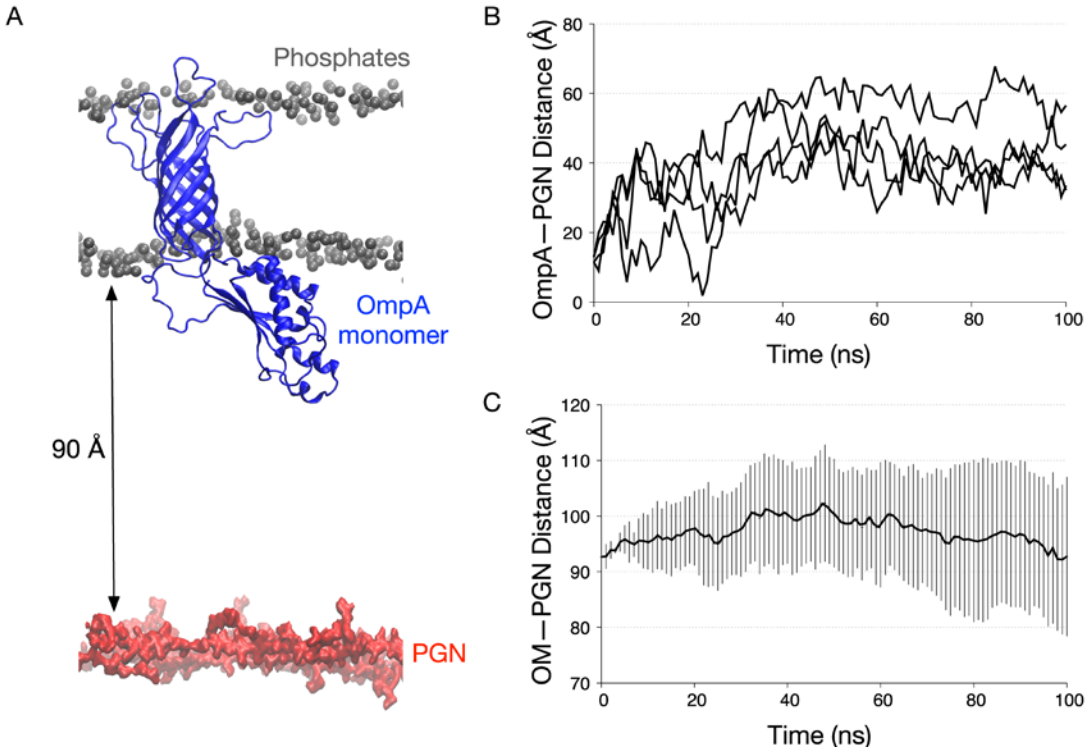

Figure 4 | OmpA monomer interactions with the OM. (A) A snapshot at the end of one of the simulations of OmpA monomer (blue) without BLP, highlighting the interactions of the CTD and the membrane (grey spheres represents the phosphorus atoms). **(B)** Minimum distance between OmpA CTD and the PGN network for all four simulations of OmpA monomer without BLP. **(C)** Distance between the PGN network and the OM measured as described in Figure 3, averaged over all four independent simulations. Error bars indicate standard deviations.

The OmpA dimer readily binds to PGN. While earlier experimental and computational work often considered OmpA as a monomer (Arora et al. 2001; Arora et al. 2000; Bond et al. 2002), evidence from several recent studies suggests that full length OmpA can form a homodimer (Stenberg et al. 2005; Zheng et al. 2011; Marcoux et al. 2014). We therefore built a similar simulation system using a model of OmpA dimer proposed by Robinson and

co-workers (Marcoux et al. 2014). In contrast to the monomer simulations, we found that the OmpA dimer was able to bind the PGN network with or without BLP. Again, the unstructured linker connecting the NTD and the CTD played an essential role in initiating PGN binding. In simulations without BLP, the linker first extended by around 15 Å compared to its original length to reach the underlying PGN sheet (Fig. 5A). Once binding occurred the linker then contracted, concomitantly shifting the PGN layer upwards by about 30 Å (Fig. 5B). While the entire PGN layer was lifted, the area around the CTD showed a more pronounced upward shift, resulting in a small undulatory pattern on the PGN surface (Fig. 5C).

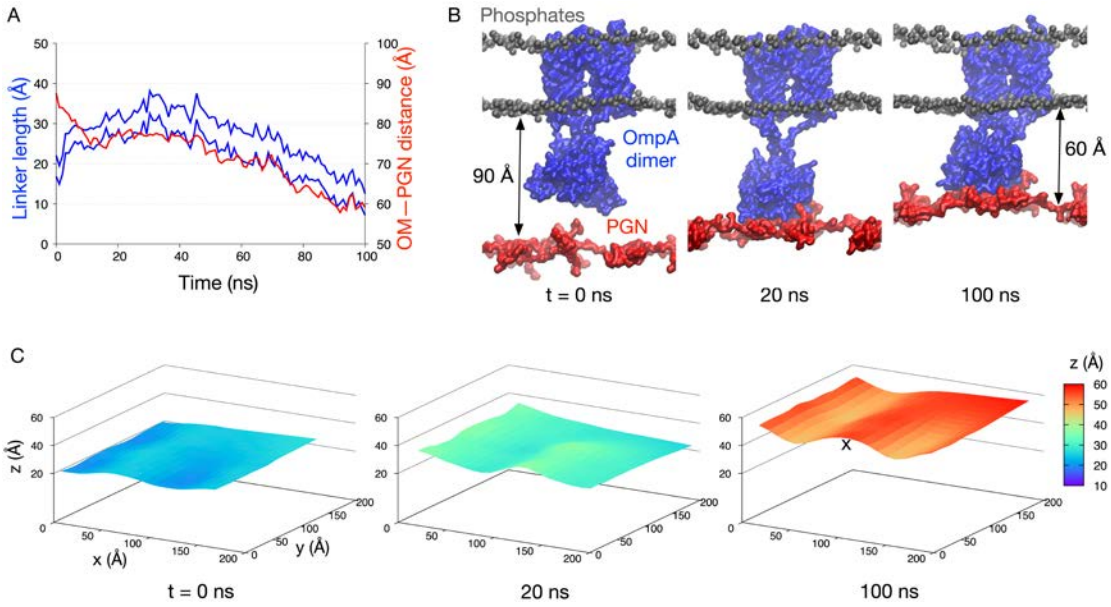

Figure 5 | OmpA dimer interactions with PGN. (A) The length of the unstructured linker connecting OmpA NTD and CTD (blue), plotted against the distance between the PGN network and the OM (red) for one of the simulations of OmpA dimer without BLP. The former is measured as previously described (Ortiz-Suarez et al. 2016), while the latter is measured as in Figure 3. **(B)** Snapshots of this simulation at three different time points, highlighting the interactions between OmpA CTD (blue) and PGN network

(red). **(C)** The z-coordinates of the PGN network projected into a surface representation at these three time points to illustrate undulations observed during the simulations. “x” indicates a local buckling effect induced by interactions with OmpA CTD.

We have previously shown that the linker regions of the OmpA dimer in the absence of BLP are quite flexible; with the ability to extend and contract without disrupting the secondary structure of either the N- or C-terminal domains (Ortiz-Suarez et al. 2016; Samsudin et al. 2016). In the present simulations, comparing the systems with and without BLP, we found an intriguing difference. The presence of BLP reduced the amount of extension required by the linker to initiate interactions between OmpA CTD and PGN. In simulations with the BLP, the linker extended by only around 5 Å, compared to 15 Å in OmpA only simulation (Fig. S3). This is concordant with the ability of the BLP to lift the PGN networks upwards and reduce the distance between the latter and the OmpA CTD.

Next we attempted to systematically elucidate the key residues involved in initial binding of OmpA and PGN by performing a contact analysis, combining data from simulations of both monomer and dimer (Fig. S4). Similar to the monomer simulations, a stretch of basic and polar residues, namely N203, K294, Q295 and R296, at the bottom of the CTD showed the highest degree of contacts. The latter three residues are part of a large insert only found in OmpA from certain bacteria, which comprises the least stable region of the protein as shown by a NMR study (Ishida et al. 2014) and previous

computational simulations (Samsudin et al. 2016). The lysine and arginine residues are conserved in homologs from *S. enterica* and *N. meningitides* and, based on their crystal structures, are positioned similarly compared to the ones in *E. coli* (Fig. S5) (Grizot & Buchanan 2004), suggesting a potentially conserved PGN binding mechanism in these three species.

Decomposing the non-bonded energies of the OmpA and PGN interaction into their Coulombic and Lennard-Jones components revealed that the former contributes ten times more than the latter (Figure S6), further corroborating the role of electrostatic interactions for initial binding of OmpA to PGN. Mutations of the key residues (N202, K294, Q295 and R296) to alanine indeed altered the way OmpA interacted with PGN (Figure S7). The timescale of interaction was longer with the mutant compared to wild type (50 ns instead of 10 ns). Also, instead of forming a stable binding interface involving both subunits of the CTD, only one of them contacted the underlying PGN network, suggesting that these polar and basic residues play a key role in the initial binding process. That the OmpA dimer is able to bind PGN without BLP implies that the electrostatic force from these basic residues, which is stronger than the monomer due to the dimerisation, is able to attract the oppositely charged PGN network over the timescale of the current simulations.

OmpA CTD binds to the BLP. The periplasm is a crowded environment with myriad proteins surrounding the PGN cell wall. In addition to OmpA interacting with PGN, it is also likely that the ubiquitous BLP molecules make contact with OmpA. We therefore examined our simulation trajectories for such

interactions and found that in three out of four dimer simulations and in one out of four monomer simulations, BLP interacted with OmpA. In all of these simulations, the BLP helices played a key role in contacting the OmpA CTD while the BLP lipid tails remained further away from the OmpA NTD (Figs. 6A and 6B). This form of interactions involving only the helical part of the BLP and not the lipidated region was possible due to the tilted configuration adopted by the BLP. The higher frequency of interactions with the BLP of the OmpA dimer compared to the monomer is likely caused by the larger size of the former, which increased the possibility of OmpA to be within close proximity of the BLP.

Delineating the key residues for OmpA-BLP interactions was more challenging due to the different ways the OmpA CTD contacting the BLP helices. In most simulations, however, BLP formed multiple salt bridges with residues on OmpA. We therefore mapped the electrostatic profile of the BLP helices and found that the surface was indeed highly charged, whereby a group of basic residues clustered towards both the N- and C-termini of the helices, while the center of the helices was populated by acidic residues (Fig. 6C). This suggests that most residues on the surface of the BLP helices are able to form electrostatic interactions with OmpA CTD. To corroborate this, we performed a contact analysis and found that there was no single prominent residue responsible for this interaction, but instead most of the polar and charged residues in the middle of the helices showed a high degree of contact with OmpA (Fig. 6D). Our results therefore suggest that BLP and OmpA CTD are able to form non-specific electrostatic interactions in the periplasm.

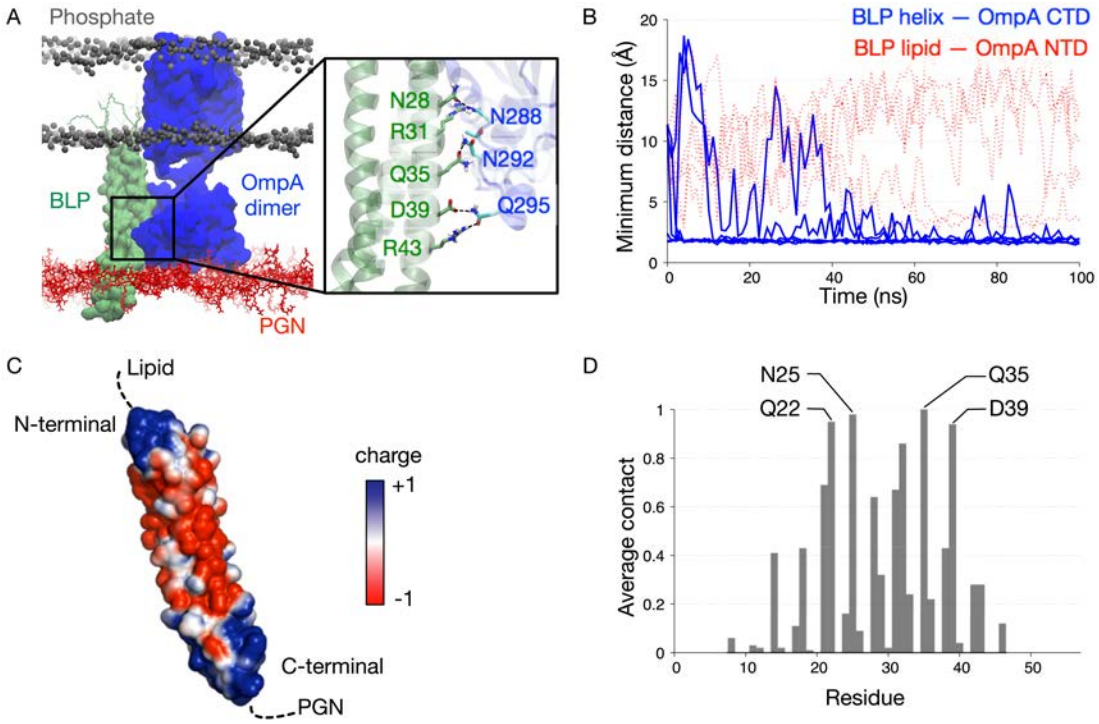

Figure 6 | OmpA interactions with BLP. (A) A snapshot at the end of one of the simulations of OmpA dimer (blue) with BLP (green), highlighting their interactions. Enlarged image shows residues involved in these interactions from both proteins. **(B)** Minimum distance between the BLP helices and the OmpA CTD for all simulations of OmpA dimer shown in blue, while the minimum distance between the BLP lipid tails and the OmpA NTD shown in red dashed lines. **(C)** Electrostatic profile of the BLP calculated using APBS (Baker et al. 2001) in PyMol (DeLano 2002). **(D)** Contact analysis performed for each residue of the BLP averaged over all simulations where OmpA-BLP interactions were observed. A score of 1 indicate contacts throughout the entire 100 ns simulations. A distance cut-off of 4 Å was used for this analysis.

Discussion

We have constructed an atomistic model of the *E. coli* OM bound to a network of PGN molecule via both non-covalent interactions with the outer membrane

porin OmpA, and covalent linkage with the BLP. Our simulations uncover important insights into the initial binding of OmpA with the PGN cell wall and the role of BLP in facilitating these interactions. OmpA has been shown to bind PGN in a labile manner (Samsudin et al. 2016), and therefore it is likely that the CTD is in equilibrium between PGN-bound and PGN-unbound states. We demonstrated that from the unbound state, BLP helps the binding of OmpA monomer to the PGN network by lifting the latter closer to the former. Without BLP, the CTD of the OmpA monomer binds to the lower leaflet of the OM instead on the timescale of the simulations present here. OmpA homodimer, on the other hand, can readily contact the PGN network by extending the linker between the NTD and the CTD, even in the absence of BLP. For both the monomer and dimer, binding is mediated by electrostatic interactions via several basic and polar residues, which are conserved in two other OmpA homologs from *S. enterica* and *N. meningitides* (Grizot & Buchanan 2004). Intriguingly these residues, and the mobile insert in which they are found, are not conserved in species like *A. baumannii* (Park et al. 2012), and are also absent in other OmpA-like domains such as the *E. coli* PAL (Abergel et al. 2001; Gourlay et al. 2013) and MotB (Roujeinikova 2008). This suggests that while PGN interactions in the binding pocket of OmpA-like domains is conserved across species (Park et al. 2012; Samsudin et al. 2016), the initial interactions are likely to differ owing to the different residues found on the surface of these proteins. We acknowledge that in our simulations, PGN did not make any significant contact with the two key residues in the binding pocket (Park et al. 2012), D241 and R256, most likely due to the relatively short time scale of the simulations. We note here that

much longer simulations or enhanced sampling methods are needed to allow the peptide chain on PGN to enter the binding pocket and form stable interactions with these residues.

To date, OmpA is the only integral membrane eight-stranded beta barrel protein that co-exists as both monomers and dimers (Zheng et al. 2011). While a model of the full-length homodimer has been proposed by mass spectrometry (Marcoux et al. 2014), and has been shown to interact with PGN from simulation studies (Samsudin et al. 2016) the physiological role of dimerisation is still to be confirmed. That the dimeric interface was localized within the CTD (Zheng et al. 2011; Marcoux et al. 2014) suggests a functional importance of dimerisation to the role of the CTD and its interactions with the cell wall. A homolog of OmpA CTD from *N. meningitides*, RmpM, may also exist as a dimer, as indicated by both the crystal structures and solution experiments, which the authors suggest would promote more efficient binding to PGN (Grizot & Buchanan 2004). Indeed, our OmpA dimer simulations revealed that the CTD was able to form a stable interaction with the underlying PGN layer even in the absence of the BLP. We conjecture that this is caused by the dimerisation increasing the negatively charged surface area at the bottom of the CTD, and thereby strengthening the electrostatic attraction towards the PGN network. In its monomeric form, the OmpA CTD has only half as many basic residues in this region. This weaker electrostatic attraction is inadequate to surpass the energetic penalty of extending the linker connecting the NTD and the CTD, which therefore leads to contraction of the linker and subsequently interaction of the CTD and the OM. Taken

466 together, our simulations suggest that OmpA dimerisation increases the
467 possibility of initial contact with the PGN cell wall, and therefore directly
468 contributes towards maintaining the integrity of the cell envelope.
469
470 The BLP is one of the most abundant proteins in Gram-negative bacteria;
471 whereby around 7.2 x 10^5 molecules are found within each cell (Braun &
472 Sieglin 1970). Similarly, OmpA is one of the most ubiquitous outer membrane
473 porins in *E. coli* (Smith et al. 2007). As both proteins play a critical structural
474 role in preserving the robustness of the PGN cell wall, it is highly likely that
475 BLP and OmpA function cooperatively. We show in this study that indeed BLP
476 is required for OmpA to interact with the PGN cell wall in its monomeric state.
477 In regions without BLP, OmpA forms homodimers to maintain this interaction.
478
479 We rationalize the differences between the behavior of OmpA monomer and
480 dimers in the absence of BLP as follows: there is a fine balance between the
481 energy required to extend the OmpA linker regions and the favorable
482 electrostatic interactions formed between the C terminal domain and PGN.
483 When only the monomer is present, the linker will not extend, instead the C-
484 terminal domain forms electrostatic interactions with the lower leaflet of the
485 outer membrane. In the case of the dimer, the combined C-terminal domains
486 of the two monomers now provide a larger area for electrostatic interaction
487 with PGN, and this gain in electrostatic interactions is sufficient to overcome
488 the energy barrier required to extend the linkers. This is further augmented by
489 the steric hindrance imposed by the dimerisation interface towards interaction
490 with the lower leaflet of the outer membrane (Samsudin et al. 2015).

Crucially our results uncover some of the important insights into the interplay between the molecular components of the Gram-negative bacterial cell envelope, towards a better structure-function understanding of the barrier protecting the bacteria from antibiotics.

Author Contributions

SK and FS designed the research and wrote the paper. FS and AB performed the research. TP developed the parameters for BLP attachment to the Om and helped to write portions of the paper.

Acknowledgements

We would like to acknowledge use of the Iridis 3 & 4 High Performance Computing Facilities at Southampton. FS was supported by a UK Biotechnology and Biological Sciences Research Council grant, number BB/M029573/1

References

Abergel, C. et al., 2001. Crystallization and preliminary crystallographic study of the peptidoglycan-associated lipoprotein from Escherichia coli. *Acta. Cryst. D*, 57(2), pp.317–319.

Abraham, M.J. et al., 2015. Gromacs: High performance molecular simulations through multi-level parallelism from laptops to supercomputers. *SoftwareX*, 1–2, pp.19–25.

Aibara, S. et al., 1972. Changes in Positional Distribution of Fatty Acids in the Phospholipids of Escherichia coli after Shift-Down in Temperature. *Biochim. Biophys. Acta*, 270, pp.301–306.

Appelmelk, B.J. et al., 1994. Frequencies of lipopolysaccharide core types in Escherichia coli strains from bacteraemic patients. *Microbiology*, 140(5), pp.1119–1124.

Arora, A. et al., 2000. Refolded Outer Membrane Protein A of Escherichia coliForms Ion Channels with Two Conductance States in Planar Lipid Bilayers. *J. Biol. Chem.*, 275(3), pp.1594–1600. Available at: http://www.jbc.org/content/275/3/1594.long.

Arora, A. et al., 2001. Structure of outer membrane protein A transmembrane domain by NMR spectroscopy. *Nat. Struct. Biol.*, 8(4), pp.334–8. Available at: http://www.ncbi.nlm.nih.gov/pubmed/11276254.

Baker, N.A. et al., 2001. Electrostatics of nanosystems: application to microtubules and the ribosome. *Proc. Natl. Acad. Sci. U.S.A.*, 98(18), pp.10037–41. Available at: http://www.pubmedcentral.nih.gov/articlerender.fcgi?artid=56910&tool=pmcentrez&rendertype=abstract.

Barlow, D.J. & Thornton, J.M., 1988. Helix geometry in proteins. *J. of Mol. Biol.*, 201(3), pp.601–619. Available at: http://linkinghub.elsevier.com/retrieve/pii/0022283688906419 [Accessed April 27, 2017].

Berendsen, H.J. et al., 1981. Interaction models for water in relation to protein hydration. In B. Pullman, ed. *Intermolecular Forces*. Boston: Reidel Publishing, pp. 331–342.

Bond, P.J., Faraldo-Gómez, J.D. & Sansom, M.S.P., 2002. OmpA: a pore or not a pore? Simulation and modeling studies. *Biophys. J.*, 83(2), pp.763–775.

Bosch, V. & Braun, V., 1973. Distribution of murein-lipoprotein between the cytoplasmic and outer membrane of *Escherichia coli*. *FEBS Letters*, 34(2), pp.307–310. Available at: http://doi.wiley.com/10.1016/0014-5793%2873%2980818-X [Accessed April 10, 2017].

Braun, V., 1975. Covalent lipoprotein from the outer membrane of escherichia coli. *Biochim. Biophys. Acta.*, 415(3), pp.335–377. Available at: http://www.sciencedirect.com/science/article/pii/0304415775900131.

Braun, V. & Sieglin, U., 1970. The Covalent Murein-Lipoprotein Structure of the Escherichia coli Cell Wall: The Attachment Site of the Lipoprotein on the Murein. *Eur. J. Riochem*, 13, pp.336–346. Available at: http://onlinelibrary.wiley.com/store/10.1111/j.1432-1033.1970.tb00936.x/asset/j.1432-1033.1970.tb00936.x.pdf?v=1&t=j1c21g7z&s=adb0b930cbb317460639e5135be470ccb933a29f [Accessed April 10, 2017].

Braun, V. & Wolff, H., 1970. The murein-lipoprotein linkage in the cell wall of Escherichia coli. *Eur. J. Biochem.*, 14, pp.387–391.

Bussi, G., Donadio, D. & Parrinello, M., 2007. Canonical sampling through velocity rescaling. *J. Chem. Phys.*, 126(1), p.14101. Available at: http://www.ncbi.nlm.nih.gov/pubmed/17212484 [Accessed January 13, 2014].

Cohen, E.J. et al., 2017. Nanoscale-length control of the flagellar driveshaft requires hitting the tethered outer membrane. *Science*, 356, pp.197–200.

Available at:
http://science.sciencemag.org/content/sci/356/6334/197.full.pdf
[Accessed August 3, 2017].

Dahl, A.C.E., Chavent, M. & Sansom, M.S.P., 2012. Bendix: Intuitive helix geometry analysis and abstraction. *Bioinformatics*, pp.1–2. Available at: http://www.ncbi.nlm.nih.gov/pubmed/22730430.

DeLano, W., 2002. The PyMOL molecular graphics system. Available at: http://www.pymol.org.

Deville, J., Rey, J. & Chabbert, M., 2008. Comprehensive analysis of the helix-X-helix motif in soluble proteins. *Proteins*, 72(1), pp.115–135. Available at: http://doi.wiley.com/10.1002/prot.21879 [Accessed April 27, 2017].

Essmann, U. et al., 1995. A smooth particle mesh Ewald method. *J. Chem. Phys.*, 103(19), p.8577. Available at: http://link.aip.org/link/JCPSA6/v103/i19/p8577/s1&Agg=doi [Accessed January 13, 2014].

Gourlay, L.J. et al., 2013. Exploiting the burkholderia pseudomallei acute phase antigen BPSL2765 for structure-based epitope discovery/design in structural vaccinology. *Chem. Biol.*, 20(9), pp.1147–1156.

Grizot, S. & Buchanan, S.K., 2004. Structure of the OmpA-like domain of RmpM from Neisseria meningitidis. *Mol. Microbiol.*, 51(4), pp.1027–1037.

Hess, B. et al., 1997. LINCS: A linear constraint solver for molecular simulations. *J. Comp. Chem.*, 18(12), pp.1463–1472. Available at: http://doi.wiley.com/10.1002/(SICI)1096-987X(199709)18:12%3C1463::AID-JCC4%3E3.0.CO;2-H.

Horta, B.A.C. et al., 2011. New interaction parameters for oxygen compounds in the GROMOS force field: Improved pure-liquid and solvation properties for alcohols, ethers, aldehydes, ketones, carboxylic acids, and esters. *J. Chem. Theory Comput.*, 7(4), pp.1016–1031.

Inouye, M., Shaw, J. & Shen, C., 1972. The Assembly of a Structural Lipoprotein in the Envelope of Escherichia coli. *J. Biol. Chem.*, 247(24), pp.8154–8159. Available at: http://www.jbc.org/content/247/24/8154.full.pdf [Accessed April 10, 2017].

Ishida, H., Garcia-Herrero, A. & Vogel, H.J., 2014. The periplasmic domain of Escherichia coli outer membrane protein A can undergo a localized temperature dependent structural transition. *Biochim. Biophys. Acta.*, 1838(12), pp.3014–3024. Available at: http://www.ncbi.nlm.nih.gov/pubmed/25135663.

Khalid, S. et al., 2008. OmpA: gating and dynamics via molecular dynamics simulations. *Biochim. Biophys. Acta*, 1778(9), pp.1871–80. Available at: http://www.ncbi.nlm.nih.gov/pubmed/17601489 [Accessed March 23, 2011].

Kito, M. et al., 1975. Metabolism of the phosphatidylglycerol molecular species in Escherichia coli. *Eur. J. Biochem.*, 54(1), pp.55–63.

Koebnik, R., 1995. Proposal for a peptidoglycan-associating alpha-helical motif in the C-terminal regions of some bacterial cell-surface proteins. *Mol. Microbiol.*, 16, pp.1269–1270.

Langelaan, D.N. et al., 2010. Improved Helix and Kink Characterization in Membrane Proteins Allows Evaluation of Kink Sequence Predictors. *J. Chem. Inf. Model.*, 50(12), pp.2213–2220. Available at:

http://pubs.acs.org/doi/abs/10.1021/ci100324n [Accessed April 27, 2017].

Lee, N. & Inouye, M., 1974. Outer Membrane Proteins of Eschericia coli: Biosynthesis and Assembly. *FEBS Lett.*, 39(2). Available at: http://onlinelibrary.wiley.com/store/10.1016/0014-5793(74)80043-8/asset/feb20014579374800438.pdf?v=1&t=j1c25u20&s=bebeff0c7e9d0fbddaf0f5a8945e2535dd3535c4 [Accessed April 10, 2017].

Lugtenberg, E.J.. & Peters, R., 1976. Distribution of lipids in cytoplasmic and outer membranes of Escherichia coli K12. *Biochim. Biophys. Acta*, 441(195 6), pp.38–47.

Marcoux, J. et al., 2014. Mass spectrometry defines the C-terminal dimerization domain and enables modeling of the structure of full-length OmpA. *Structure*, 22(5), pp.781–790. Available at: http://dx.doi.org/10.1016/j.str.2014.03.004.

Ortiz-Suarez, M.L. et al., 2016. Full-Length OmpA: Structure, Function, and Membrane Interactions Predicted by Molecular Dynamics Simulations. *Biophys. J.*, 111(8), pp.1692–1702. Available at: http://linkinghub.elsevier.com/retrieve/pii/S0006349516308025.

Park, J.S. et al., 2012. Mechanism of anchoring of OmpA protein to the cell wall peptidoglycan of the gram-negative bacterial outer membrane. *FASEB J.*, 26(1), pp.219–228.

Parrinello, M. & Rahman, A., 1981. Polymorphic Transitions in Single Crystals: a New Molecular Dynamics Method. *J. Appl. Phys.*, 52(12), pp.7182–7190.

Parsons, L.M., Lin, F. & Orban, J., 2006. Peptidoglycan recognition by Pal, an outer membrane lipoprotein. *Biochemistry*, 45(7), pp.2122–2128.

Pautsch, a & Schulz, G.E., 1998. Structure of the outer membrane protein A transmembrane domain. *Nat. Struct. Biol.*, 5(11), pp.1013–1017.

Piggot, T.J., Holdbrook, D.A. & Khalid, S., 2011. Electroporation of the E. coli and S. Aureus membranes: molecular dynamics simulations of complex bacterial membranes-suppinfo. *J. Phys. Chem.*

Roujeinikova, A., 2008. Crystal structure of the cell wall anchor domain of MotB, a stator component of the bacterial flagellar motor: implications for peptidoglycan recognition. *Proc. Natl. Acad. Sci. U.S.A.*, 105(30), pp.10348–53. Available at: http://www.pnas.org/content/105/30/10348.full.

Samsudin, F. et al., 2015. Accurate Prediction of Ligand Affinities for a Peptide Transporter. *Cell Chem. Biol.*, 23(2), pp.299–309.

Samsudin, F. et al., 2016. OmpA: A Flexible Clamp for Bacterial Cell Wall Attachment. *Structure*, 24(12), pp.2227–2235. Available at: http://linkinghub.elsevier.com/retrieve/pii/S0969212616303173.

Schmid, N. et al., 2011. Definition and testing of the GROMOS force-field versions 54A7 and 54B7. *Eur. Biophys. J.*, 40(7), pp.843–856.

Shu, W. et al., 2000. Core structure of the outer membrane lipoprotein from Escherichia coli at 1.9 A resolution. *J. Mol. Biol.*, 299(4), pp.1101–1112.

Silhavy, T.J., Kahne, D. & Walker, S., 2010. The bacterial cell envelope. *Cold Spring Harb. Perspect. Biol.*, 2(5), pp.1–17.

Smith, S.G.J. et al., 2007. A molecular Swiss army knife: OmpA structure, function and expression. *FEMS Microbiol. Lett.*, 273(1), pp.1–11.

Stenberg, F. et al., 2005. Protein complexes of the Escherichia coli cell envelope. *J. Biol. Chem.*, 280(41), pp.34409–34419.

Tsirigos, K.D., Bagos, P.G. & Hamodrakas, S.J., 2011. OMPdb: a database of beta-barrel outer membrane proteins from Gram-negative bacteria. *Nucleic Acids Res.*, 39, pp.D324-31. Available at: http://www.ncbi.nlm.nih.gov/pubmed/20952406 [Accessed April 28, 2017].

Vinogradov, E. V. et al., 1999. The structures of the carbohydrate backbones of the lipopolysaccharides from Escherichia coli rough mutants F470 (R1 core type) and F576 (R2 core type). *Eur. J. Biochem.*, 261(3), pp.629–639.

Vollmer, W. & Bertsche, U., 2008. Murein (peptidoglycan) structure, architecture and biosynthesis in Escherichia coli. *Biochim. Biophys. Acta.*, 1778(9), pp.1714–1734.

Vollmer, W., Blanot, D. & De Pedro, M.A., 2008. Peptidoglycan structure and architecture. *FEMS Microbiology Reviews*, 32(2), pp.149–167.

Vollmer, W., Höltje, J. & Ho, J., 2004. The Architecture of the Murein (Peptidoglycan) in Gram-Negative Bacteria: Vertical Scaffold or Horizontal Layer(s)? *J. Bacteriol.*, 186(18), pp.5978–5987.

Wolf, M.G. et al., 2010. g_membed : Efficient Insertion of a Membrane Protein into an Equilibrated Lipid Bilayer with Minimal Perturbation. *J. Comp. Chem.*, 31(11), pp.2169–2174.

Yokota, K., Kanamoto, R. & Kito, M., 1980. Composition of cardiolipin molecular species in Escherichia coli. *J. Bacteriol.*, 141(3), pp.1047–1051.

Zheng, C. et al., 2011. Cross-linking measurements of in vivo protein complex topologies. *Mol. Cell Proteomics*, 10(10), p.M110.006841.

690